A NEW NUMERICAL METHODOLOGY FOR COMPUTATIONAL FLUID DYNAMICS FRAMED WITHIN THE BOND GRAPH THEORY

Jorge Luis Baliño
Instituto de Pesquisas Energéticas e Nucleares (IPEN), Av. Prof. Lineu Prestes, 2242 - Cidade Universitária,
CEP 05508-00, São Paulo, SP, Brazil
jlbalino@ipen.br

Abstract. This paper shows distinctive features and some results obtained with a new numerical methodology for Computational Fluid Dynamics (CFD), which is the result of the right combination of Bond Graph concepts with elements of Numerical Methods. This methodology was used so far to model single-phase, single-component and single-phase, multicomponent flows. The main characteristics of this new methodology, called BG-CFD, are summarized. Some results of one-dimensional, single-component problems corresponding to heat conduction, convection-diffusion and compressible flows are discussed, showing that this methodology is a foundation of a bridge between Bond Graphs and CFD.
Keywords. CFD, Computational Fluid Dynamics, Bond Graphs, Numerical Methods.

1. Introduction

1.1. Bond Graphs and CFD

In order to solve multidimensional problems with the aid of computer programs, it is important that these models can be implemented numerically. This task, main concern of the area of Computational Fluid Dynamics (CFD), is performed by systematically discretizing the continua, that is, by replacing the continuous variables by a combination of a finite set of nodal values and interpolating functions. The result is a (generally nonlinear) algebraic approximation, instead of the original differential or integro-differential problem.

The Bond-Graph formalism allows for a systematic approach for representing and analyzing dynamic systems (Karnopp *et al.*, 2000). Dynamic systems belonging to different fields of knowledge, like Electrodynamics, Solid Mechanics or Fluid Mechanics, can be described in terms of a finite number of variables and basic elements.

In the field of Fluid Dynamics, the potential benefits of Bond Graphs have not been yet fully exploited. The applications made so far dealt with problem restrictions such as the neglect of inertia terms (which amounts for the major non-linearities), very simple flow geometries or the use of the so-called "pseudo bond graphs". Besides, the applications to fluid dynamic systems were not oriented to a systematic spatial discretization of flow fields, typical of CFD problems.

The first attempt to apply Bond Graphs to CFD problems appeared in (Fahrenthold & Venkataraman, 1996), although the formulation was restricted to prescribed shape functions and nodalization. Besides, heat conduction (which leads to convection-diffusion problems) was not modeled.

It is well known that the Bond Graph representation depicts in a very elegant way the conservation of energy in the various forms in which it may appear in a given dynamic, lumped-parameter system. The definition of suitable generalized effort and flow variables, based on the system total energy, allows to obtain the state equations in an orderly fashion.

1.2. Motivation

In a previous work (Baliño *et al.*, 2001) a theoretical development of a new methodology for CFD in a single-phase, single-component flow was presented, which is a result of the right combination of Bond Graph concepts with elements of numerical methods. This methodology, called BG-CFD, was successfully applied to one-dimensional convection-diffusion (Gandolfo *et al.*, 2001) and compressible problems (Gandolfo *et al.*, 2002). In other contributions (Baliño, 2001b; Baliño, 2002), it was shown that BG-CFD includes Control Volumes and Finite Differences as particular cases of the linearized state equations. Recently, BG-CFD was extended to single-phase, multicomponent flows (Baliño, 2003a; Baliño, 2003b). The motivation of this paper is to show distinctive features and some results obtained so far with this methodology. The mathematical expressions shown in this paper correspond to the single-phase, single-component flow problem.

2. The BG-CFD Methodology

2.1. Definition of the Independent Variables

Since BG-CFD is a power conserving approach, it is essential to have a representation of the total energy per unit volume $e_v^* = u_v + t_v^*$, where u_v is the internal energy per unit volume and $t_v^* = \frac{1}{2}\rho V^2$ is the kinetic coenergy per unit volume. We choose the density ρ, the entropy per unit volume s_v and the velocity V as the independent variables. From this representation, the power balance per unit volume can be written as:

$$\frac{\partial e_v^*}{\partial t} = (\psi + \kappa)\frac{\partial \rho}{\partial t} + \theta \frac{\partial s_v}{\partial t} + p_v . \frac{\partial V}{\partial t} \tag{1}$$

where t is the time, and:

$$\psi = \frac{1}{\rho}(u_v + P - \theta s_v) = \left(\frac{\partial u_v}{\partial \rho}\right)_{s_v} \quad ; \quad \kappa = \frac{1}{2} V^2 = \left(\frac{\partial t_v^*}{\partial \rho}\right)_V \quad ; \quad \theta = \left(\frac{\partial u_v}{\partial s_v}\right)_\rho \quad ; \quad p_v = \rho V = \left(\frac{\partial t_v^*}{\partial V}\right)_\rho \tag{2}$$

In Eq. (1) and (2) ψ is the Gibbs free energy per unit mass, κ is the kinetic coenergy per unit mass, θ is the absolute temperature and p_v is the linear momentum per unit volume; in Eq. (2), P is the absolute pressure.

The terms that multiply the time derivatives of the independent variables can be regarded as potentials, which play the role of constitutive relations needed to close the problem. This potentials are not independent functions, but their mixed partial derivatives are related through the Maxwell relations of Thermodynamics (Callen, 1960).

An alternative formulation can be derived by taking p_v instead of V as independent variable. In this case, the formulation would be symmetric, in a sense that the volume integrals of the independent variables would result in the system mass, linear momentum and entropy. Nevertheless, we choose the velocity because it is more popular as discretized variable and because the resulting expressions are easier to calculate.

The feasibility of presenting the total energy as a sum of product of potentials times time derivatives of independent variables is not a trivial issue. In the field of Turbulence (Wilcox, 2000), for instance, the dynamics is formulated in terms of time-averaged variables and fluctuations. In the field of Multiphase Flow (Drew & Passman, 1999), the average process is more sophisticated because, besides turbulent effects within each phase, the position of the interfaces is not known, resulting in variables such as the void fraction or the interfacial area per unit volume. A representation of the mean total energy for these problems would be very useful.

2.2. Balance Equations

The balance equations are power equations (per unit volume) corresponding to each one of the terms that contributes to the time derivative of the total energy per unit volume, Eq. (1). The balance equations can be obtained starting from the conservation equations (mass, mechanical energy, thermal energy) (Whitaker, 1977) and the constitutive relations, resulting:

$$(\psi + \kappa)\frac{\partial \rho}{\partial t} = -\nabla.[\rho(\psi + \kappa)V] + \rho V.\nabla\psi + \rho V.\nabla\kappa \tag{3}$$

$$\theta \frac{\partial s_v}{\partial t} = -\nabla.(q + \theta s_v V) + \rho\Phi - \rho V.\nabla\psi + V.\nabla P + \nabla V : \underline{\underline{\tau}} \tag{4}$$

$$p_v . \frac{\partial V}{\partial t} = \nabla.(\underline{\underline{\tau}}.V) + \rho G.V - V.\nabla P - \nabla V : \underline{\underline{\tau}} - \rho V.\nabla\kappa \tag{5}$$

where q is the heat flux, Φ is the heat source per unit mass and $\underline{\underline{\tau}}$ is the viscous stress tensor.

One of the key issues in modeling fluid dynamic systems with inertial, viscous, compressible and thermal effects is the right understanding of the transformation of the different forms of energy (mechanical, thermal) and the generation of irreversibility. The balance equations show one of the advantages of this methodology, that is, the representation of the power structure of the system. In the balance equations there can be identified three type of terms: divergence, source and coupling terms. The divergence terms take into account the power introduced in the system through the boundary conditions. The source terms constitute the different power sources, external to the system. Finally, the coupling terms represent power transfer between the velocity, mass and entropy equations; these coupling terms appear, with opposite signs, in pairs of balance equations. Taking into account Eq. (1) it verifies that coupling terms cancel out when the balance equations are added, resulting:

$$\frac{\partial e_v^*}{\partial t} = \nabla.[(u_v + P + \rho\kappa)V] + \nabla.(\underline{\underline{\tau}}.V) - \nabla.q + \rho G.V + \rho\Phi \tag{6}$$

The cancellation of the coupling terms means that they influence the distribution among the power terms of Eq. (1) but not the total power in the system.

2.3. Discretization of the Flow Fields

In order to formulate the discrete model of the fluid continuum in the domain Ω, it is necessary to specify the description of the flow fields corresponding to the independent variables. In BG-CFD this is done, in the same fashion as in Finite Elements, in terms of a finite set of nodal values and interpolation functions. With this only restriction, we are free to choose different types of grids. Assuming n_ρ density nodes, n_s entropy nodes and n_V velocity nodes, we have:

$$\rho(\boldsymbol{r},t)=\sum_{k=1}^{n_\rho} \rho_k(t)\,\varphi_{\rho k}(\boldsymbol{r})=\underline{\rho}^T.\underline{\varphi_\rho}\ ;\ s_v(\boldsymbol{r},t)=\sum_{l=1}^{n_s} s_{vl}(t)\,\varphi_{sl}(\boldsymbol{r})=\underline{s_v}^T.\underline{\varphi_s}\ ;\ \boldsymbol{V}(\boldsymbol{r},t)=\sum_{l=1}^{n_V} \boldsymbol{V}_m(t)\,\varphi_{Vm}(\boldsymbol{r})=\underline{\boldsymbol{V}}^T.\underline{\varphi_V} \tag{7}$$

where $\boldsymbol{r}$ is the position, $\underline{\rho}$, $\underline{s_v}$ and $\underline{\boldsymbol{V}}$ are time-dependent nodal vectors, while $\underline{\varphi_\rho}$, $\underline{\varphi_s}$ and $\underline{\varphi_V}$ are the corresponding position-dependent nodal vectors of interpolation or shape functions. Based on this definition, we define the nodal vectors of mass $\underline{m}$ and entropy $\underline{S}$ as:

$$\underline{m}=\underline{\underline{\Omega_\rho}}.\underline{\rho}\quad ;\quad \underline{S}=\underline{\underline{\Omega_s}}.\underline{s_v}\quad ;\quad \underline{\underline{\Omega_\rho}}=(\Omega_\rho)_{kn}=\int_\Omega \varphi_{\rho k}\,\delta_{kn}\,d\Omega\quad ;\quad \underline{\underline{\Omega_s}}=(\Omega_s)_{ln}=\int_\Omega \varphi_{sl}\,\delta_{ln}\,d\Omega \tag{8}$$

where $\underline{\underline{\Omega_\rho}}$ and $\underline{\underline{\Omega_s}}$ are correspondingly diagonal volume matrices associated to the density and entropy per unit volume.

The system mass m and entropy S are related to these nodal vectors as follows:

$$m=\int_\Omega \rho\,d\Omega=\sum_{k=1}^{n_\rho} m_k\quad ;\quad S=\int_\Omega s_v\,d\Omega=\sum_{l=1}^{n_s} S_l \tag{9}$$

2.4. System Power Balance

Since the nodal vectors of mass and entropy are proportional to the nodal vectors of discretized variables, it is possible to write the system total energy E^* as:

$$E^*=U(\underline{m},\underline{S})+T^*(\underline{m},\underline{\boldsymbol{V}})\quad ;\quad U=\int_\Omega u_v\,d\Omega\quad ;\quad T^*=\int_\Omega t_v^*\,d\Omega \tag{10}$$

where U and T^* are correspondingly the system internal energy and system kinetic coenergy. The kinetic coenergy can be written as a bilinear form, involving the inertia matrix $\underline{\underline{M}}$, as:

$$T^*=\frac{1}{2}\underline{\boldsymbol{V}}^T.\underline{\underline{M}}.\underline{\boldsymbol{V}}\quad ;\quad \underline{\underline{M}}=(M)_{mn}=\int_\Omega \varphi_{Vm}\,\varphi_{Vn}\,d\Omega \tag{11}$$

Analogously to the power per unit volume, Eq. (1), the system power can be expressed as:

$$\dot{E}^*=(\underline{\Psi}-\underline{K}^T.\underline{\boldsymbol{V}}).\dot{\underline{m}}-\underline{\Theta}^T.\dot{\underline{S}}+\underline{\boldsymbol{p}}^T.\dot{\underline{\boldsymbol{V}}} \tag{12}$$

where $\underline{\Psi}$, $\underline{K}$, $\underline{\Theta}$ and $\underline{\boldsymbol{p}}$ are correspondingly nodal vectors of Gibbs free energy per unit mass, kinetic coenergy per unit mass, absolute temperature and linear momentum, defined as:

$$\underline{\Psi}=\left(\frac{\partial U}{\partial \underline{m}}\right)_{\underline{S}}=\underline{\underline{\Omega_\rho}}^{-1}.\left[\int_\Omega \psi\,\underline{\varphi_\rho}\,d\Omega\right]\quad ;\quad \underline{K}=\underline{\underline{\Omega_\rho}}^{-1}.\left[\int_\Omega \kappa\,\underline{\varphi_\rho}\,d\Omega\right] \tag{13}$$

$$\underline{\Theta}=\left(\frac{\partial U}{\partial \underline{S}}\right)_{\underline{m}}=\underline{\underline{\Omega_s}}^{-1}.\left[\int_\Omega \theta\,\underline{\varphi_s}\,d\Omega\right]\quad ;\quad \underline{\boldsymbol{p}}=\left(\frac{\partial T^*}{\partial \underline{\boldsymbol{V}}}\right)_{\underline{m}}=\underline{\underline{M}}.\underline{\boldsymbol{V}}=\int_\Omega \boldsymbol{p}_v\,\underline{\varphi_V}\,d\Omega \tag{14}$$

According to Eq. (14), the nodal vector of linear momentum can be regarded as a system volume integral of the local values weighted by the velocity interpolation function. It can be easily shown that the system linear momentum can be obtained as

$$\boldsymbol{p}=\int_\Omega \boldsymbol{p}_v\,d\Omega=\sum_{k=1}^{n_\rho} \boldsymbol{p}_k \tag{15}$$

The potentials appearing in Eq. (12) define, as in the continuous case, constitutive relations corresponding to the discrete or lumped-parameter problem; these potentials also satisfy the Maxwell relations.

It can also be shown that the volume integrals of the left side terms of Eq. (3) to (5) can be calculated as:

$$\int_\Omega \left(\psi+\kappa\,\frac{\partial \rho}{\partial t}\right)d\Omega=(\underline{\Psi}-\underline{K})^T.\dot{\underline{m}}\quad ;\quad \int_\Omega \theta\,\frac{\partial s_v}{\partial t}\,d\Omega=\underline{\Theta}^T.\dot{\underline{S}}\quad ;\quad \int_\Omega \boldsymbol{p}_v.\frac{\partial \boldsymbol{V}}{\partial t}\,d\Omega=\underline{\boldsymbol{p}}^T.\dot{\underline{\boldsymbol{V}}} \tag{16}$$

2.5. State Equations

The system state equations are obtained by integrating in volume the balance equations, Eq. (3) to (5). The expressions for the system state equations are:

$$\dot{\underline{m}}=\dot{\underline{m}}_M^{(r)}-\dot{\underline{m}}_{ev}-\dot{\underline{m}}_{ch}-\dot{\underline{m}}_K \tag{17}$$

$$\dot{\underline{S}}=\dot{\underline{S}}_Q^{(r)}-\dot{\underline{S}}_{ev}-\dot{\underline{S}}_{ch}-\dot{\underline{S}}_{\Gamma}-\dot{\underline{S}}_P+\dot{\underline{S}}_D \tag{18}$$

$$\dot{\underline{\boldsymbol{V}}}=\underline{\underline{M}}^{-1}.\left(\underline{\boldsymbol{F}}_{\Gamma}^{(r)}-\underline{\boldsymbol{F}}_{ch}-\underline{\boldsymbol{F}}_{\Gamma}-\underline{\boldsymbol{F}}_D-\underline{\boldsymbol{F}}_K\right) \tag{19}$$

The different terms in the system state equations (17) to (19) arise from integrations over the domain volume Ω or the domain boundary Γ. Their definitions are:

$$\underline{\dot{m}_W^{(\Gamma)}} = -\left(\underline{\underline{\Psi}} + \underline{\underline{K}}\right)^{-1}.\left[\int_\Gamma \underline{w_\rho}\,\rho\,(\psi+\kappa)V.\check{n}\,d\Gamma\right] \;;\; \underline{\dot{m}_{WF}} = \left(\underline{\underline{\Psi}} + \underline{\underline{K}}\right)^{-1}.\left[\int_\Omega \rho\,(\psi+\kappa)V.\nabla \underline{w_\rho}\,d\Omega\right] \tag{20}$$

$$\underline{\dot{m}_U} = \left(\underline{\underline{\Psi}} + \underline{\underline{K}}\right)^{-1}.\left[\int_\Omega \underline{w_\rho}\,\rho V.\nabla\psi\,d\Omega\right] \;;\; \underline{\dot{m}_K} = \left(\underline{\underline{\Psi}} + \underline{\underline{K}}\right)^{-1}.\left[\int_\Omega \underline{w_\rho}\,\rho V.\nabla\kappa\,d\Omega\right] \tag{21}$$

$$\underline{\dot{S}_{QF}^{(\Gamma)}} = -\underline{\underline{\Theta}}^{-1}.\left[\int_\Gamma \underline{w_s}\,(\boldsymbol{q}+\theta\, s_v V).\check{n}\,d\Gamma\right] \;;\; \underline{\dot{S}_{WF}} = \underline{\underline{\Theta}}^{-1}.\left[\int_\Omega (\boldsymbol{q}+\theta\, s_v V).\nabla \underline{w_\rho}\,d\Omega\right] \tag{22}$$

$$\underline{\dot{S}_F} = \underline{\underline{\Theta}}^{-1}.\left[\int_\Omega \underline{w_s}\,\rho\,\Phi\,d\Omega\right] \;;\; \underline{\dot{S}_U} = \underline{\underline{\Theta}}^{-1}.\left[\int_\Omega \underline{w_s}\,\rho V.\nabla\psi\,d\Omega\right] \tag{23}$$

$$\underline{\dot{S}_P} = \underline{\underline{\Theta}}^{-1}.\left[\int_\Omega \underline{w_s}\,V.\nabla P\,d\Omega\right] \;;\; \underline{\dot{S}_D} = \underline{\underline{\Theta}}^{-1}.\left[\int_\Omega \underline{w_s}\,(\nabla V:\underline{\underline{\tau}})d\Omega\right] \tag{24}$$

$$\underline{F_T^{(\Gamma)}} = \int_\Gamma \left(\underline{\underline{\tau}}.\check{n}\right)\underline{\varphi_V}\,d\Gamma \;;\; \underline{F_G} = \int_\Omega \rho\,\boldsymbol{G}\,\underline{\varphi_V}\,d\Omega \;;\; \underline{F_P} = \int_\Omega \nabla P\,\underline{\varphi_V}\,d\Omega \tag{25}$$

$$\underline{F_D} = \int_\Omega \underline{\underline{\tau}}.\nabla \underline{\varphi_V}\,d\Omega \;;\; \underline{F_K} = \int_\Omega \rho\nabla\kappa\,\underline{\varphi_V}\,d\Omega \tag{26}$$

In Eq. (20) to (26) diagonal matrices are defined, whose elements are the components of the nodal vectors $\underline{\Psi}$, $\underline{K}$ and $\underline{\Theta}$:

$$\underline{\underline{\Psi}} = (\Psi)_{kn} = \Psi_k\,\delta_{kn} \;;\; \underline{\underline{K}} = (K)_{kn} = K_k\,\delta_{kn} \;;\; \underline{\underline{\Theta}} = (\Theta)_{ln} = \Theta_l\,\delta_{ln} \tag{27}$$

In Eq. (20) to (24), $\underline{w_\rho}$ and $\underline{w_s}$ are nodal vectors of weight functions corresponding to density and entropy per unit volume; these weight functions are introduced to satisfy the power interchanged by the system through the boundaries, as well as to share the importance of the power terms, appearing in the balance equations, among neighboring nodes. In the discretization procedure, each component of the right side terms of the mass balance equation and entropy balance equation were multiplied correspondingly by $w_{\rho k}$ and w_{sl} before integrating in volume; although this procedure has the advantage that the steady-state balance equations are satisfied locally for the different nodes, other strategies are possible and should be investigated. It will be shown later how these weight functions can be used to handle the upwind nature of the fluid equations. It is interesting to notice that no weight functions are needed for the velocity state equations.

It is clear that the resulting state equations, which are non-linear, are obtained following a different approach than in other numerical methods. Although they are used nodal values and interpolation and weight functions, which could resemble what is done in the Finite Element Method, the state equations are not obtained from a minimization of any functional. The state equations are not obtained either from any scheme like the ones used in Finite Differences. Finally, the state variables do not correspond to the integrated variables in a control volume, except for the particular case of uniform (unity) interpolation functions.

The state equations are different from the ones obtained with other popular numerical methods. The main characteristic of this methodology is the conservation of different power flows in the system, while the system mass, linear momentum and entropy can be calculated as the sum of the corresponding nodal values.

2.6. Boundary and Initial Conditions

All kind of boundary conditions are handled consistently through the terms representing surface integrals ($\underline{\dot{m}_W^{(\Gamma)}}$, $\underline{\dot{S}_{QF}^{(\Gamma)}}$ and $\underline{F_T^{(\Gamma)}}$). Initial conditions can be defined by readily specifying the nodal values of the states variables as:

$$\underline{m}(t=0) = \underline{m_0} \;;\; \underline{S}(t=0) = \underline{S_0} \;;\; \underline{V}(t=0) = \underline{V_0} \tag{28}$$

Alternatively, if spatial functions for density, velocity and entropy per unit volume are specified for the initial time, the nodal values must be determined in order to conserve the system mass, linear momentum and entropy, resulting:

$$\underline{m_0} = \int_\Omega \rho(\boldsymbol{r},t=0)\,\underline{\varphi_\rho}\,d\Omega \;;\; \underline{S_0} = \int_\Omega s_v(\boldsymbol{r},t=0)\,\underline{\varphi_s}\,d\Omega \;;\; V_{0m} = \frac{\int_\Omega \rho(\boldsymbol{r},t=0)V(\boldsymbol{r},t=0)\varphi_{V_m}\,d\Omega}{\int_\Omega \rho(\boldsymbol{r},t=0)\varphi_{V_m}\,d\Omega} \tag{29}$$

2.7. Coupling Matrices

The coupling terms appearing in the balance equations shown in Section 2.2, when integrated in volume, give raise to power terms that can be expressed as the product of different pairs of nodal vectors. Since these power terms are

conserved, there must be a relationship between the nodal vector involved. The representation of these relationships is performed through the coupling matrices.

It can be shown that the coupling terms appearing in the velocity and mass state equations set the following relationships:

$$\underline{\dot{m}_K} = \underline{\underline{M_{MV}}} \cdot \underline{V} \quad ; \quad \underline{F_K} = \underline{\underline{M_{MV}}}^T \cdot (\underline{\Psi} + \underline{K}) \quad ; \quad \underline{\underline{M_{MV}}} = (M_{MV})_{km} = \frac{1}{\Psi_k + K_k} \left[\int_\Omega w_{\rho k} \varphi_{Vm} \rho \nabla \kappa \, d\Omega \right] \tag{30}$$

where $\underline{\underline{M_{MV}}}$ is a rectangular matrix (n_ρ rows and n_v columns). For the coupling terms appearing in the entropy and mass state equations, the relationships are:

$$\underline{\dot{m}_K} = \underline{\underline{M_{MS}}} \cdot \underline{\Theta} \quad ; \quad \underline{\dot{S}_U} = \underline{\underline{M_{MS}}}^T \cdot (\underline{\Psi} + \underline{K}) \quad ; \quad \underline{\underline{M_{MS}}} = (M_{MS})_{kl} = \frac{1}{\Psi_k + K_k} \frac{1}{\Theta_l} \left[\int_\Omega w_{\rho k} \varphi_{sl} \rho V \cdot \nabla \psi \, d\Omega \right] \tag{31}$$

where $\underline{\underline{M_{MS}}}$ is a rectangular matrix (n_ρ rows and n_s columns). Finally, for the coupling terms appearing in the velocity and entropy state equations, the relationships are:

$$\underline{F_P} + \underline{F_D} = \underline{\underline{M_{SV}}} \cdot \underline{\Theta} \quad ; \quad \underline{\dot{S}_P} + \underline{\dot{S}_D} = \underline{\underline{M_{SV}}}^T \cdot \underline{V} \quad ; \quad \underline{\underline{M_{SV}}} = (M_{SV})_{ml} = \frac{1}{\Theta_l} \left[\int_\Omega w_{sl} \left(\nabla P \, \varphi_{Vm} - \underline{\underline{\tau}} \cdot \nabla \varphi_{Vm} \right) d\Omega \right] \tag{32}$$

where $\underline{\underline{M_{SV}}}$ is a rectangular matrix (n_V rows and n_s columns).

Since the coupling matrices are not inversible, they set restrictions on the allowable input nodal vectors. It can be seen in Eq. (30) to (32) that the nodal vectors of mass rate and entropy rate are output variables.

3. System Bond Graph

Although no mention was made so far in the presentation of BG-CFD, the methodology was developed based on the Bond Graph theory. The power structure of the system can be depicted very elegantly in the Bond Graph shown in Fig. 1; through this figure, various concepts and drawing conventions can be introduced.

In the Bond Graph shown in Fig. 1, there can be identified different elements with ports connected by bonds, which are drawn as arrows. In each bond we have a pair of generalized effort and flow variables. The bond orientation indicates the direction of power flow when the inner product of these variables is positive. In addition, the effort variable is represented to the side of the bond inclined stroke.

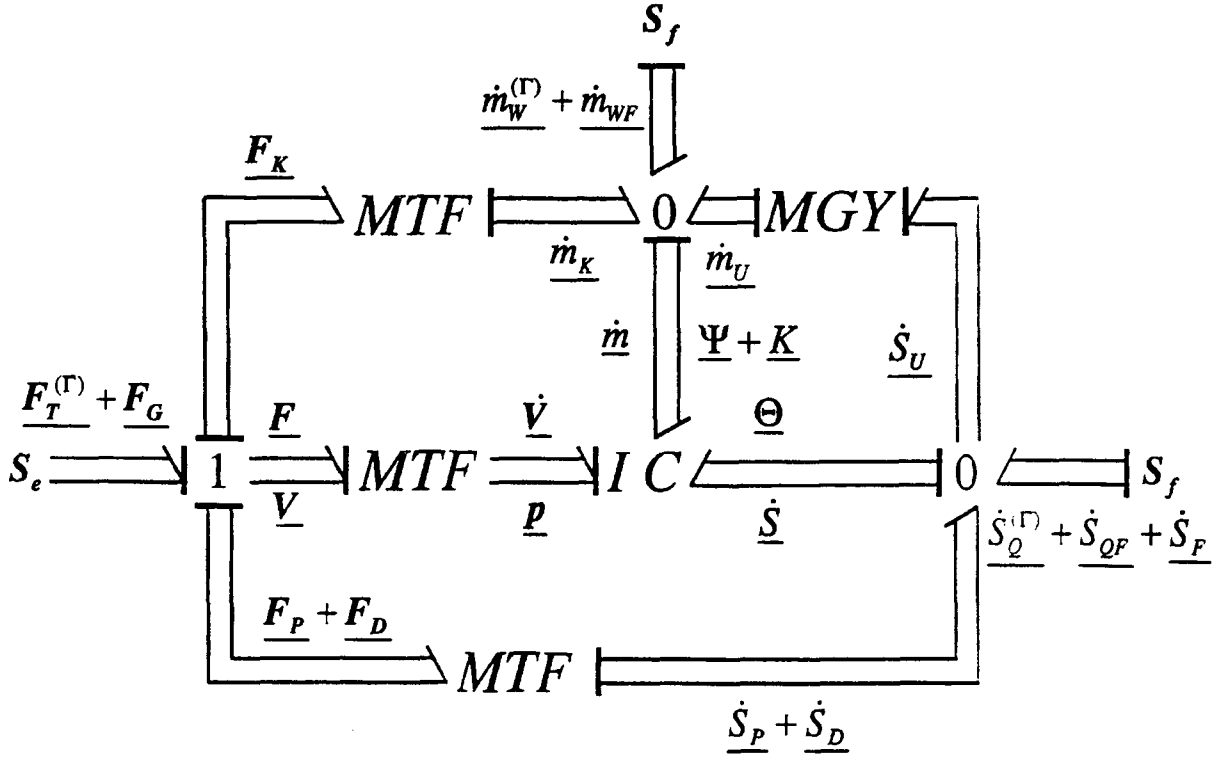

Figure 1. System Bond Graph for a single-component, single-phase flow.

The representation of the system total energy E^* as an exact differential of the state variables $\underline{m}$, $\underline{S}$ and $\underline{V}$ define an energy-storing element known as multibond *IC*-field (drawn as ***IC***); this field has a inertial port and two capacitive ports, representing the system power flows due correspondingly to velocity, mass and entropy rates, as seen in Eq. (12).

The effort variables are $\underline{\dot{V}}$, $\underline{\Psi} + \underline{K}$ and $\underline{\Theta}$, while the corresponding flow variables are $\underline{p}$, $\underline{\dot{m}}$, and $\underline{\dot{S}}$; according to the graph, the power flows in the field when the product of any pair of variables is positive.

A modulated multibond transformer (drawn as ***MTF***) is connected to the inertial port of the *IC*-field. A transformer is a power conserving element characterized by a relation between the flow variables at both sides (in this case $\underline{p}$ and $\underline{V}$) such as shown in Eq. (14), in which the inertia matrix $\underline{\underline{M}}$ (dependent on the mass nodal vector) is the transformer modulus. Since power is conserved through a transformer, the relationship between the corresponding effort variables is $\underline{\dot{V}} = \underline{\underline{M}}^{-1} . \underline{\boldsymbol{F}}$. Notice that the inertia matrix is always inversible.

A common flow, or multibond 1-junction (drawn as **1**) is used to represent the velocity state equation, Eq. (19). In a 1-junction, the flow (in this case $\underline{V}$) is the same for all bonds, and the corresponding effort (in this case, the different forces) are algebraically added.

A common effort, or multibond 0-junction (drawn as **0**), connected to the capacitive (entropy) port of the *IC*-field, is used to represent the entropy state equation, Eq. (18). In a 0-junction, the effort (in this case $\underline{\Theta}$) is the same for all bonds, and the corresponding flows (in this case, the different entropy rates) are algebraically added.

Another multibond 0-junction (drawn as **0**), connected to the capacitive (mass) port of the *IC*-field, is used to represent the mass state equation, Eq. (17); $\underline{\Psi} + \underline{K}$ is the same for all bonds, and the corresponding mass rates are algebraically added.

Modulated sources are used to represent the terms coming from boundary conditions (integrals over the system boundary Γ), as well as other source terms. There exist effort and flow sources: in each case, either the effort or flow is a given function, independent of the power supplied or absorbed. In the velocity state equation, a modulated multibond effort source (drawn as $\boldsymbol{S}_e$) is used to represent the forces $\underline{\boldsymbol{F}_T^{(\Gamma)}} + \underline{\boldsymbol{F}_G}$. In the entropy and mass state equations, modulated flow sources (drawn as $\boldsymbol{S}_f$) are used to represent correspondingly the entropy rates $\underline{\dot{S}_Q^{(\Gamma)}} + \underline{\dot{S}_{QF}} + \underline{\dot{S}_F}$ and the mass rates $\underline{\dot{m}_W^{(\Gamma)}} + \underline{\dot{m}_{WF}}$.

The power couplings between the velocity and mass state equations, Eq. (30), and between the velocity and entropy state equations, Eq. (32), are also represented by modulated multibond transformers, in which the corresponding coupling matrices are the transformer moduli.

Finally, the power coupling between the entropy and mass state equations, Eq. (31), is represented by a modulated multibond gyrator. A gyrator is a power conserving element characterized by a relation between the effort and flow variables at both sides, in which the coupling matrix is the gyrator modulus.

A very important feature of Bond Graphs is the concept of causality. The causality is drawn at one end of a bond as a perpendicular stroke, which indicates the direction in which the effort is directed; this is, the effort is an input variable to the port connected to the bond end with the causal stroke. By implication, the flow is an input variable to the port connected to a bond end that does not have a causal stroke. Once the Bond Graph of a system is drawn, there exist a sequential procedure for causality assignment, after which each bond has only one causal stroke and the elements have possible causalities; for instance, an effort source has only one possible causality, so the causal stroke must be always at the opposite end of the bond connected to the source. The causality assignment allows to choose a set of state variables and assures that the problem is mathematically well-posed. The resulting causality is shown in Fig. 1; it is interesting to see that the restrictions imposed by the coupling matrices are satisfied.

4. Some results

4.1. Comparison with other Numerical Methods

In (Baliño, 2001b ; Baliño, 2002) BG-CFD was applied to one-dimensional compressible, viscous flow with heat transfer. It was considered a one-dimensional discretization, as shown in Fig. 2, in which the mass, entropy and velocity nodes are coincident (not staggered).

It is interesting to consider a uniform distribution (this is, constant piecewise shape functions) of the independent variables, because these are the simplest and because the state variables correspond to the mass, entropy and velocity within the control volumes bounded by the lines located midway between the grid points. For the first and last nodes, half control volumes are defined. With the assumptions made above, the inertia matrix becomes diagonal and the state equations corresponding to the different nodal state variables can be obtained analytically.

The discontinuities present in the description of the flow fields are handled through the use of distributional derivatives (Kanwal, 1998), this is, derivatives involving delta functions. In calculating the different terms corresponding to the state equations, there must be taken into account the continuous contributions, as well as the distributional contributions. The distributional contributions are located at the discontinuity surfaces of the independent variables and weight functions. Since the profiles of the independent variables are constant piecewise, all the terms involving spatial derivatives only have distributional contributions.

It is interesting to find out whether such simple shape functions can model viscous effects and heat conduction. Calculating the terms involving the viscous stress tensor, it can be shown that viscous effects cannot be taken into

account with a constant velocity shape function, this is, $\underline{F_T^{(r)}} = \underline{F_D} = \underline{0}$ and $\underline{\dot{S}_D} = \underline{0}$; at least a linear velocity profile is needed to model viscous effects. On the other hand, it can be shown that heat conduction can be modeled with constant shape functions if the gradient of the entropy weight functions is nonzero at the discontinuity surfaces. Consequently, it was shown that the choice of the shape and weight functions is related to the physical effects that can be rigorously modeled with this methodology.

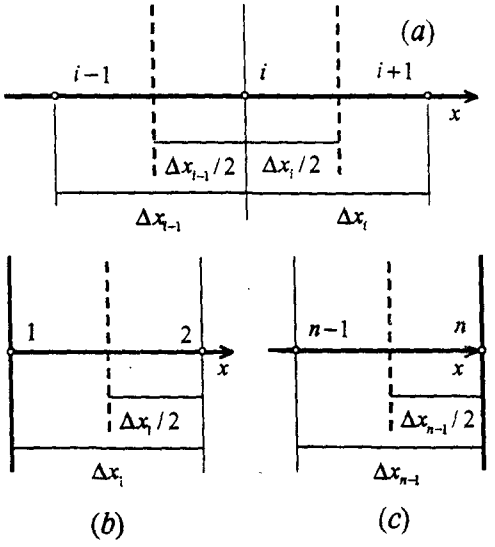

Figure 2. Discretization for: (*a*) an inner node, (*b*) first node and (*c*) last node.

Based on the Second Principle of Thermodynamics, there were investigated restrictions on the entropy weight functions by considering heat conduction in two reservoirs of thermal energy at different temperatures, that are allowed to communicate through a thermal resistance but are thermally insulated from the surroundings at the rest of the surfaces. It was shown that it is also necessary for the entropy weight functions to decrease with respect to the distance to the corresponding entropy nodes.

There were also written linearized expressions of the state equations obtained with this discretization, which are valid for problems with small space changes of the state variables and can be compared to the resulting expressions obtained from other numerical methods, such as Control Volumes or Finite Differences.

In the Control Volume approach (Patankar, 1980), the calculation domain is divided into a number of overlapping control volumes such that there is one control volume surrounding each grid point. The differential equations are then integrated over each control volume, assuming convenient (in general different) profiles for evaluating the flux, source and unsteady terms. It was found that the density and entropy weight functions evaluated at the control volume boundaries can be regarded as weight factors in the calculation of the corresponding fluxes, while the gradient of the entropy weight function evaluated at the control volume boundaries come out to be proportional to the weight factors in the calculation of the conductive entropy fluxes. The limit values (1 or 0) for the mass and entropy weight functions evaluated at the boundaries corresponds to the full upwind conditions.

In the Finite Difference approach (Tannehill *et al.*, 1997), the derivatives in the differential equations are replaced by truncated Taylor-series expansions. Expressions coincident with the ones obtained by using this formulation can be obtained with the appropriate choice of the weight functions evaluated at the discontinuities. In this case, the limit values (1 or 0) for the mass and entropy weight functions evaluated at the boundaries corresponds to the forward or backward approximation for the derivatives.

As a consequence, BG-CFD includes the Control Volume and Finite Difference methods as particular cases, obtaining an interpretation of the density and entropy weight functions appearing in the methodology. In Sections 4.2 and 4.3 there are shown simple schemes to determine these functions.

4.2. Convective-Diffusive Flows

An interesting type of CFD problems are those in which heat transport is due to heat conduction and fluid flow. These situations define what are known as convection-diffusion problems (Patankar, 1980). The main characteristic of such problems is that the velocity field and the density are given.

In (Gandolfi *et al.*, 2001) BG-CFD was applied to convection-diffusion problems. In the resulting Bond Graph, which is a simplification of the one shown in Fig. 1, there is power flow only at the entropy port and, since the velocity field is known, all the terms in the entropy state equation are represented by generalized flow sources.

One-dimensional examples of heat conduction and convection-diffusion problems were presented, and the results were compared to the analytical ones. For simplicity, it was assumed incompressible flow with constant velocity and thermophysical properties, as well as a uniform grid spacing. Piecewise constant shape functions and piecewise linear

weight functions were assumed for the entropy, as shown in Fig. 3. In these figure, x is a local coordinate with origin at the entropy node l and β is a parameter independent of position, which must be optimized in order to satisfy a specified condition, regarding the accuracy of the numerical solution; the analysis for this optimization is deferred to Section 4.2.2.

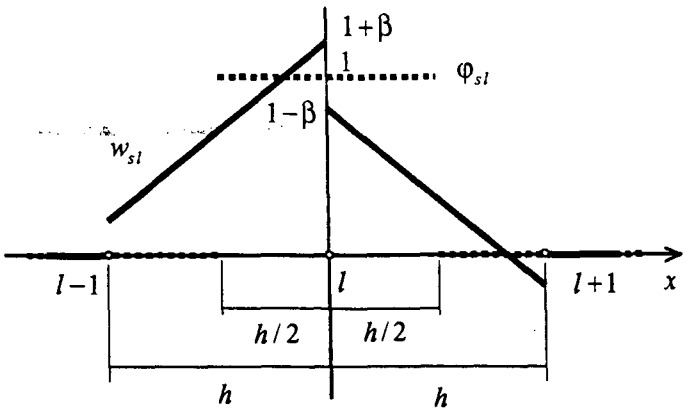

Figure 3. Shape and weight functions for an inner node (the weight function is shown in a continuous line).

4.2.1. Heat Conduction

For heat conduction, the reference velocity is zero and the resulting state equations are independent of β. In Fig. 4 there are presented numerical results for heat conduction, without heat sources ($\Phi = 0$), in the slab $0 \le x \le L$, with boundary and initial conditions:

$$\frac{\partial \theta}{\partial x}(0,t) = 0 \quad ; \quad -\lambda \frac{\partial \theta}{\partial x}(L,t) = H\left[\theta(L,t) - \theta_\infty\right] \quad ; \quad \theta(x,0) = \theta_0 \tag{33}$$

In Eq. (33), λ is the thermal conductivity and H is the heat transfer coefficient , while θ_∞ and θ_0 are reference temperatures. The numerical and exact solutions (Carslaw & Jaeger, 1959) for the nondimensional temperature as a function of $x^* = \frac{x}{L}$, are compared in terms of the following nondimensional parameters:

$$\hat{\theta} = \frac{\theta - \theta_\infty}{\theta_0 - \theta_\infty} \quad ; \quad Bi = \frac{H L}{\lambda} \quad ; \quad Fo = \frac{\alpha_\theta t}{L^2} \quad ; \quad \alpha_\theta = \frac{\lambda}{\rho c_v} \tag{34}$$

where Bi and Fo are correspondingly the Biot and Fourier numbers, while α_θ, ρ and c_v are correspondingly the thermal diffusivity, the density and the constant volume specific heat.

The numerical results shown in Fig. 4 correspond to a fairly large number of nodes ($n_s = 201$); this has been done on purpose to show that the formulation is indeed spatially consistent. Although good accuracy was also obtained with much coarser grids, this particular problem is very tough for uniform grids, due to the steep temperature profiles that appear for $Fo << 1$.

4.2.2. Convection-Diffusion

Results are presented for the convection-diffusion problem in the region $0 \le x \le L$, with boundary and initial conditions:

$$\theta(0,t) = \theta_0 \quad ; \quad \theta(L,t) = \theta_L \quad ; \quad \theta(x,0) = \theta_0 \tag{35}$$

The analytical solution for $\hat{\theta} = \frac{\theta - \theta_L}{\theta_0 - \theta_L}$ are also dependent on the Peclet number $Pe_L = \frac{\rho c_v U L}{\lambda}$, while the behavior of the numerical solution is dependent on the grid Peclet number $Pe_h = \frac{\rho c_v U h}{\lambda}$.

For $\beta = 0$ the properties are evenly weighted, resulting the centered scheme. The solution show a known behavior: for grid Peclet numbers greater than a critical value ($Pe_{hc} = 2$), the numerical results present oscillations and are no longer a good approximation of the analytical solution. These oscillations can be observed in Fig. 5, for the steady state solution.

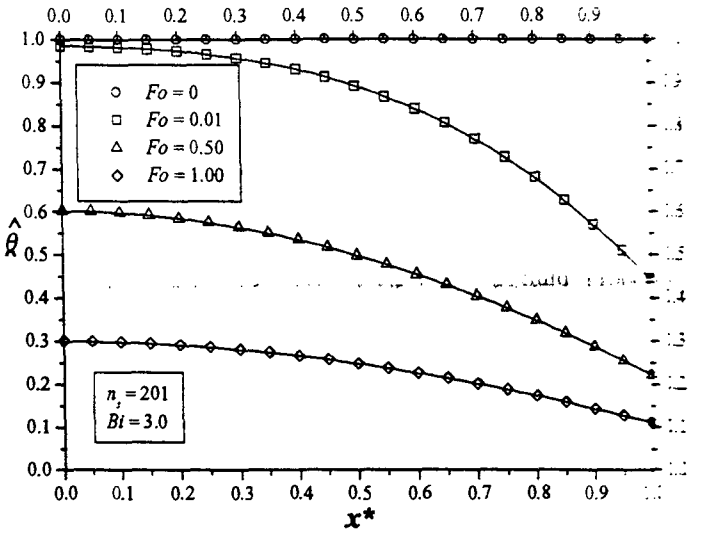

Figure 4. Heat conduction in a slab. Analytical solutions are shown in continuous lines, while calculated values are shown for selected nodes.

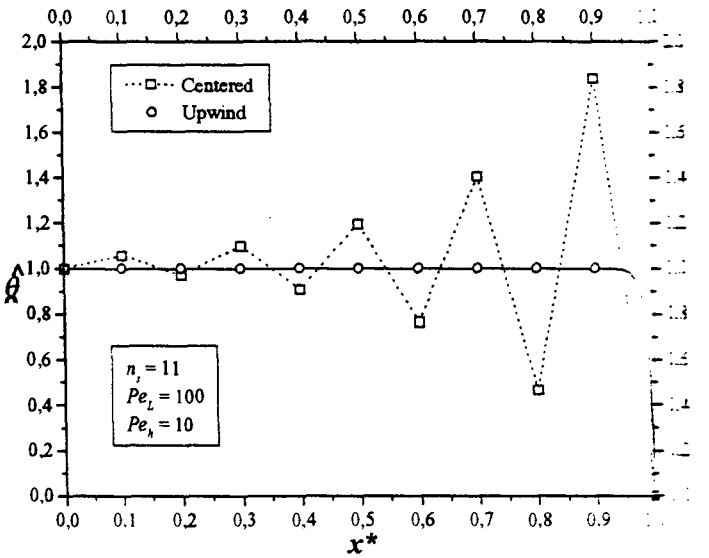

Figure 5. Convection-diffusion in a slab, steady state. Linear weight function, upwind. The analytical solution is shown in a continuous line.

A remedy for these unrealistic oscillations in the solution obtained with the linear weight function in convection-diffusion problems is the introduction of upwind schemes. Upwind schemes basically weight unevenly the convected properties corresponding to the points located upstream, compared to the points located downstream.

For advection-diffusion problems, upwind schemes can be introduced naturally by means of the weight functions. It was proposed to perform an optimization of the parameter β by setting the condition that the numerical scheme has to give the exact steady state value for the entropy at the node I for given values of the entropy at the nodes $I-1$ and $I+1$. This approach is loosely related to others used in Finite Element Methods (Hughes, [17]). The calculation gives:

$$\beta = -\frac{1}{Pe_h} + \frac{1}{2}\frac{\exp(Pe_h)+1}{\exp(Pe_h)-1} \tag{36}$$

It can be verified that β is an antisymmetric function, with the asymptotic values $\mp\frac{1}{2}$ for $Pe_h \to \pm\infty$. For $\beta = \frac{1}{2}$, the properties located downstream have no influence in the integration, and viceversa. With the optimal value of β it was observed that the solutions obtained are all consistent, even for very high Peclet numbers, as shown in Fig. 5.

4.3 Compressible Flows

In (Gandolfo *et al.*, 2002) BG-CFD was used to solve the so called "shock tube" problem (Emanuel, 1986). The problem is depicted in Fig. 6. The tube, of length $L = 1\,m$ and a cross section of $0.01\,m^2$, has been discretized into 100 equal sections ($n_\rho = n_s = n_v = 101$). Concerning the shape functions, piecewise constant were adopted for density and entropy, while continuous linear were adopted for velocity, in order to be able to model viscous effects. As weight functions, linear piecewise were adopted for the entropy, similar to the ones shown in Fig. 3, while linear continuous were adopted for the density. No-flow and adiabatic boundary conditions were specified at both ends. The following fluid properties for air -taken from (Fahrenthold & Venkataraman, 1996)- were used: reference temperature $\theta_0 = 273\,K$, reference density $\rho_0 = 1.2955\,kg\,m^{-3}$, viscosity $\mu = 1.7153\ 10^{-5}\,Pa\,s$, constant volume specific heat $c_v = 718\,J\,kg^{-1}\,K^{-1}$.

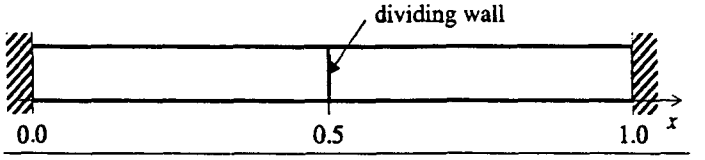

Fig. 6. The shock tube.

The domain is initially separated in two sections by a solid wall located at $x = 0.5\,m$. The gas is at rest in both sections, and the initial density and total entropy conditions at the left section are $\rho = \rho_0$ and $S = 0$, while for the right section are $\rho = \frac{1}{2}\rho_0$ and $S = 4.4247\,J\,K^{-1}$. At $t = 0$ the solid wall is ruptured, generating a shock wave travelling to the right and a rarefaction wave travelling to the left.

The resulting state equations were solved with a time step $\Delta t = 1.3\ 10^{-5}\,s$. As it is usual (Fahrenthold & Venkataraman, 1996; Sod, 1978; Monaghan & Gingold, 1983) an artificial viscosity was introduced, in order to damp the numerical oscillations at the wave fronts. The numerical and analytical results for the density, entropy per unit mass, velocity and pressure at $t = 0.001s$ are shown in Fig. 7 to 10.

Comparing the numerical and analytical solutions, it can be seen that there is a reasonable agreement, being the numerical results a bit diffusive because of the artificial viscosity. Although more work would be needed in the selection of weight and shape functions, the simple ones chosen in this work have shown to be adequate for dealing with a complex nonlinear problem involving all physical effects.

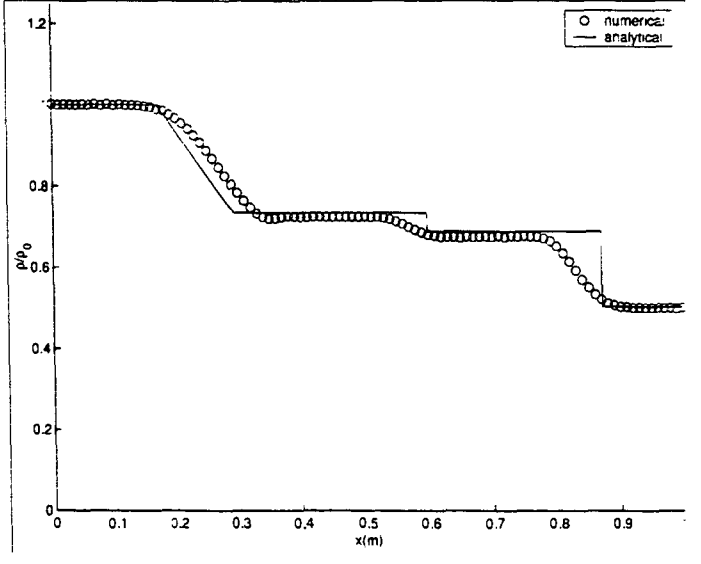

Fig. 7. Non-dimensional density at $t = 0.001s$, shock-tube problem.

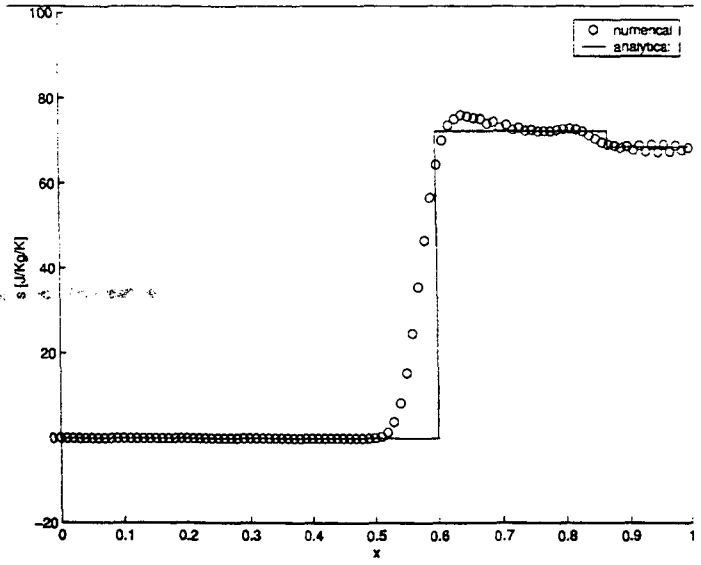

Fig. 8. Entropy per unit mass at $t = 0.001s$, shock-tube problem.

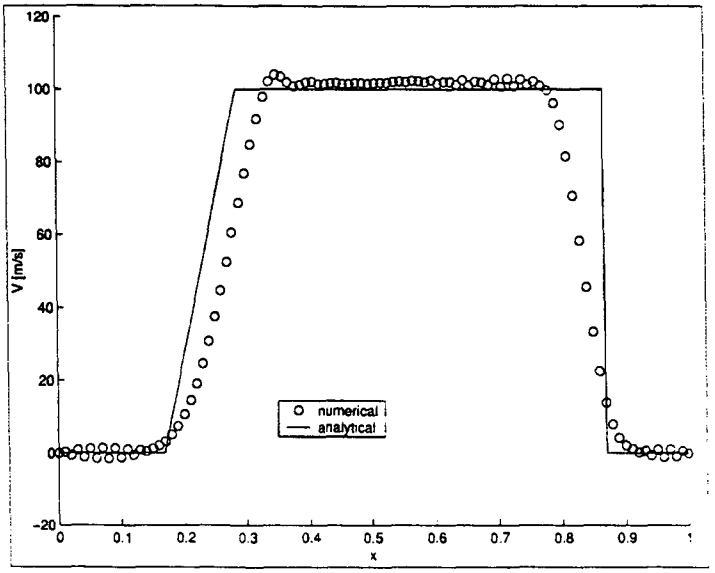

Fig. 9. Velocity at $t = 0.001s$, shock-tube problem.

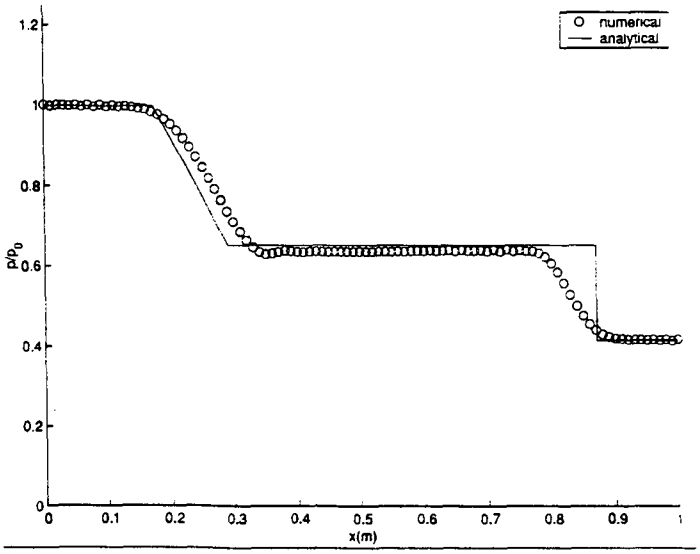

Fig. 7. Non-dimensional pressure at $t = 0.001s$, shock-tube problem.

5. Conclusions

Distinctive features of a new methodology for CFD based on the Bond Graph theory were presented, as well as results obtained so far in convection-diffusion and compressible flow problems. This methodology is focused on the power structure of the system, offering a new perspective to solve CFD problems. It is hoped that these findings encourage other researchers to use this formalism in more complex problems.

Acknowledgment

The author wishes to thank Conselho Nacional de Desenvolvimento Científico e Tecnológico (CNPq, Brazil) for the financial support as Visiting Researcher at IPEN.

6. References

Baliño, J. L., Larreteguy, A. E. & Gandolfo, E. F., 2001, "A General Bond Graph Approach for Computational Fluid Dynamics. Part I: Theory", 2001 International Conference on Bond Graph Modeling and Simulation (ICBGM '2001) (in CD and Proceedings), The Society for Computer Simulation, pp. 41-46. ISBN 1-56555-221-0), Phoenix, Arizona, USA.

Baliño, J. L., 2001b, "Bond-Graph Formulation of CFD Problems with Constant Piecewise Shape Functions", VII International Seminar on Recent Advances in Fluid Mechanics, Physics of Fluids and Associated Complex Systems (Fluidos'2001) (in CD, ISBN 987-20148-0-9), Buenos Aires, Argentina.

Baliño, J. L., 2002, "Bond-Graph Approach for Computational Fluid Dynamics: a Comparison with other Numerical Methods", Second IEEE International Conference on System, Man and Cybernetics (SMC'02)}, Paper TAB13 (in CD, IEEE No. 02CH37349C, ISBN 0-7803-7438-X), Hammamet, Tunisia.

Baliño, J. L., 2003a, "BG-CFD Methodology for Multicomponent Solutions. Part I: Multivelocity Model", 2003 International Conference on Bond Graph Modeling and Simulation (ICBGM'2003), Orlando, Florida, USA.

Baliño, J. L., 2003b, "BG-CFD Methodology for Multicomponent Solutions. Part II: Diffusion Model", 2003 International Conference on Bond Graph Modeling and Simulation (ICBGM'2003), Orlando, Florida, USA.

Callen, H. B., 1960, "Thermodynamics", John Wiley & Sons, Inc., ISBN 0-471-13036-2.

Carslaw, H. S. & Jaeger, J. C., 1959, "Conduction of Heat in Solids", Second Edition, Oxford University Press, ISBN 0-19-853368-3, 510 p.

Drew, D. A. & Passman, 1999, S. L., "Theory of Multicomponent Fluids", Springer-Verlag, New York, Inc., ISBN 0-387-98380-5, 308 p.

Emanuel G., 1986, "Gasdynamics: Theory and Applications", AIAA Education Series, New York, 1986.

Fahrenthold, E. P. & Venkataraman, M., 1996, "Eulerian Bond Graphs for Fluid Continuum Dynamics Modeling", ASME Journal of Dynamic Systems, Measurement, and Control, Vol. 118, pp. 48-57.

Gandolfo, E. F., Larreteguy, A. E. & Baliño, J. L., 2001, "A General Bond Graph Approach for Computational Fluid Dynamics. Part II: Applications", 2001 International Conference on Bond Graph Modeling and Simulation (ICBGM '2001) (in CD and Proceedings), The Society for Computer Simulation, pp. 47-52. ISBN 1-56555-221-0), Phoenix, Arizona, USA.

Gandolfo, E. F., Larreteguy, A. E. & Baliño, J. L., 2002, "Bond-Graph Modeling of 1-D Compressible Flows", Second IEEE International Conference on System, Man and Cybernetics (SMC'02), Paper TAB14 (in CD, IEEE No. 02CH37349C, ISBN 0-7803-7438-X), Hammamet, Tunisia.

Hughes, T. J. R., 1978, "A simple scheme for developing upwind finite elements, Int. Journal for Numerical Methods in Engineering, Vol. 12, pp. 1359-1365, 1978.

Kanwal, R. P., 1998, "Generalized Functions: Theory and Technique", Birkhäuser, ISBN 0-8176-4006-1, 462 p.

Karnopp, D. C., Margolis, D. L. & Rosenberg, R. C., 2000, "System Dynamics. Modeling and Simulation of Mechatronic Systems", 3d Ed., Wiley Interscience, ISBN 0-471-33301-8, 507 p.

Monaghan, J. J. & Gingold, R. A., 1983, "Shock Simuation by the Particle Method SPH", Journal of Computational Physics, Vol. 52, pp. 373-389.

Patankar, S. V., 1980, "Numerical Heat Transfer and Fluid Flow", Hemisphere Publishing Corporation, ISBN 0-07-048740-5, 197 p.

Sod, G. A., 1978, "A Survey of Several Finite Difference Methods for Systems of Nonlineal Hyperbolic Conservation Laws", Journal of Computational Physics, Vol. 27, pp. 1-31.

Tannehill, J. C., Anderson, D. A. & Pletcher, R. H., 1997, "Computational Fluid Mechanics and Heat Transfer". Taylor & Francis, ISBN 1-56032-046-X, 792 p.

Whitaker, S., 1977, "Fundamental Principles of Heat and Mass Transfer", Pergamon Press Inc., ISBN 0-08-017866-9, 556 p.

Wilcox, D. C., 2000, "Turbulence Modeling for CFD", 2nd. Edition, DCW Industries, Inc., California, USA, ISBN 0-9636051-5-1, 540 p.

IPEN/CNEN-SP
BIBLIOTECA
"TEREZINE ARANTES FERRAZ"

Formulário de envio de trabalhos produzidos pelos pesquisadores do IPEN para inclusão na Produção Técnico Científica

---

AUTOR(ES) DO TRABALHO:
Balino, J. L.

LOTAÇÃO: CENT RAMAL: 9285/262

TIPO DE REGISTRO:

art. / periód.:	☐	Publ. IPEN	☐	. resumo	☐
cap. de livro	☐	Art. conf	☒	outros (folheto, relatório, etc...)	☐

TITULO DO TRABALHO:
A new numerical methodology for computational fluid dynamics framed within the bond graph theory!

APRESENTADO EM: (informar os dados completos - no caso de artigos de conf., informar o título da conferência, local, data, organizador, etc..)
Proceedings of COBEM 2003)

PALAVRAS CHAVES PARA IDENTIFICAR O TRABALHO:
CFD, Computational Fluid Dynamics, Bond Graphs, Numerical methods.

ASSINATURA: Cida

DATA: 08/12/2003

12 DEZ 2003